Nanoparticles carrying fingolimod and methotrexate enables targeted induction of apoptosis and immobilization of invasive thyroid cancer

Niemelä, Erik; Desai, Diti; Niemi, Rasmus; Doroszko, M; Özliseli, Ezgi; Kemppainen, Kati; Rahman, N; Sahlgren, Cecilia; Törnquist, Kid; Eriksson, John; Rosenholm, Jessica

Published in:
European Journal of Pharmaceutics and Biopharmaceutics

DOI:
10.1016/j.ejpb.2019.12.015

Published: 01/03/2020

Document Version
Accepted author manuscript

Document License
CC BY-NC-ND

Nanoparticles carrying fingolimod and methotrexate enables targeted induction of apoptosis and immobilization of invasive thyroid cancer

Niemelä E[a,f], Desai D[b], Niemi R[a], Doroszko M[c,d], Özliseli E[b], Kemppainen K[a], Rahman NA[c], Sahlgren C[a,f], Törnquist K[a,e], Eriksson JE[a,f*], Rosenholm JM[b,f*]

[a]*Cell biology, Faculty of Science and Engineering, Åbo Akademi University, Turku, Finland. E-mail: john.eriksson@abo.fi*
[b]*Pharmaceutical Sciences Laboratory, Faculty of Science and Engineering, Åbo Akademi University, Turku, Finland. E-mail: jessica.rosenholm@abo.fi*
[c]*Institute of Biomedicine, University of Turku, Finland*
[d]*Department of Immunology, Genetics and Pathology, Section for Neuro-oncology, Uppsala University, Sweden*
[e]*Minerva Foundation Institute for Medical research, Biomedicum, Helsinki, Finland.*
[f]*Turku Bioscience Centre, University of Turku and Åbo Akademi University, Turku, Finland.*

**Correspondence addressed to: jessica.rosenholm@abo.fi, +358-22153255, john.eriksson@abo.fi, +358-22153313*

Metastatic tumors are the main cause of cancer-related death as the invading cancer cells disrupt normal functions of distant organs and are nearly impossible to eradicate by traditional cancer therapeutics. This is of special concern when the cancer has created multiple metastases and extensive surgery would be too dangerous to execute. Therefore, combination chemotherapy is often the selected treatment form. However, drug cocktails often have severe adverse effects on healthy cells, whereby the development of targeted drug delivery could minimize side-effects of drugs and increase the efficacy of the combination therapy. In this study, we utilized the folate antagonist methotrexate (MTX) as targeting ligand conjugated onto mesoporous silica nanoparticles (MSNs) for selective eradication of folate receptor-expressing invasive thyroid cancer cells. The MSNs was subsequently loaded with the drug fingolimod (FTY720), which has previously been shown to efficiently inhibit proliferation and invasion of aggressive thyroid cancer cells. To assess the efficiency of our carrier system, comprehensive *in vitro* methods were employed; including flow cytometry, confocal microscopy, viability assays, invasion assay, and label-free imaging techniques. The *in vitro* results show that MTX-conjugated and FTY720-loaded MSNs potently attenuated both the proliferation and invasion of the cancerous thyroid cells while keeping the off-target effects in normal thyroid cells reasonably low. For a more physiologically relevant *in vivo* approach, we utilized the chick chorioallantoic membrane (CAM) assay showing decreased invasive behavior of the thyroid derived xenografts and an increased necrotic phenotype compared to tumors that received the free drug cocktail. Thus, the developed multidrug-loaded MSNs effectively induced apoptosis and immobilization of invasive thyroid cancer cells, and could potentially be used as a carrier system for targeted drug delivery for the treatment of diverse forms of aggressive cancers that expresses folate receptors.

Keywords: targeted drug delivery, methotrexate, fingolimod, surface functionalization, folate receptor, mesoporous silica nanoparticles, combination chemotherapy, thyroid cancer, Chicken chorioallantoic membrane.

Introduction

Cancer is one of the main causes of death in the western world nowadays. Based on an estimation from 2018, there will be over 9 million cancer-related deaths annually and over 18 million new cancer cases worldwide [1,2]. To be able to target cells of interest is one of the key aims in medicine today, as it could minimize side effects of drugs and potentially improve the success rates of different treatments [3–5]. This is highly important in cancer therapeutics, where the treatment can have serious side effects on the patient, especially in the case of metastatic cancers where the invasion of cancerous cells towards healthy organs is the main cause of cancer-related death [6,7]. Therefore, efficient targeted therapy is paramount when the cancer has created multiple metastases and extensive surgery is too dangerous for the patient for being a plausible treatment option [8,9]. In the case of multi-organ distant metastases of differentiated thyroid cancer the estimated five-year survival rate is as low as 15.3% compared to 77.6% in patients with single-organ metastasis originated from the thyroid gland [10]. Conventional chemotherapy that relies on inducing DNA damage have diverse side effects ranging from hair loss, weight loss, anemia and nausea to organ problems as the drug is systematically administered where it affects cells that are under constant renewal throughout the whole body [11–13]. Therefore, by loading a carrier system capable of targeted drug delivery towards multiple metastases using combination chemotherapeutic drugs, it could be possible to achieve synergistic effects with significantly fewer side effects on healthy cells compared to freely administered drug cocktail [14,15].

To confirm potential enhanced anti-cancerous efficacy of the carrier system in a more clinically relevant setting while keeping the cost at a reasonable level the chick chorioallantoic membrane (CAM) assay was utilized for the *in vivo* studies [16]. The CAM assay has received increased interest in the field of cancer

research and drug development during the last decades, as the tumors are easily accessible for experimental manipulation and because the chick embryo is naturally immunodeficient, supporting the inoculation of both normal and cancerous cells [17]. This makes the CAM assay an exceptionally useful model system for investigating cancer cell behavior such as tumor growth, invasion, angiogenesis and the remodeling of the surrounding tissue [16,18–20].

In the present study, we exploited the tendency of cancer cells to overexpress folate receptors (FR) on the cell membrane for folate mediated targeted delivery in order to increase the drug uptake in the FR-expressing thyroid cancer cells compared to normal thyroid cells [14,21–25]. Target selectivity was achieved by functionalizing mesoporous silica nanoparticles (MSNs) with the folate antagonist named methotrexate (MTX) that have been used in decades for chemotherapy. The drug MTX efficacy relies on blocking the DNA synthesis of fast-dividing cancer cells leading towards cell death [26,27]. In this manner, we created a targeted drug delivery system that has an efficacy by itself, opening up the possibility to load the carrier particle with a second active molecule that would further increase the efficacy of the treatment. The MSN were thus loaded with the anti-proliferating molecule fingolimod (FTY720) that works by inhibiting the phosphorylation of sphingosine and thereby blocks the production of the bioactive molecule sphingosine 1-phosphate (S1P), which is an important signaling lipid for cell growth, survival, migration, and metastasis [28,29]. By blocking the production of S1P by targeted drug delivery, metastatic cancer cells would be halted and pushed towards apoptosis [30]. Thus, we envisioned that this multidrug-loaded nanoparticle could be used for advanced metastatic cancer therapeutics where conventional treatments would often be ineffective and could potentially have severe consequences for the patient (Scheme 1) [1–7,31].

MSNs were chosen due to their unique possibility of conjugating MTX on the surface of the particle combined with high loading capabilities of poorly water-soluble drugs within the mesoporous structure, for potentially achieving enhanced and selective apoptosis in target cells [32]. In order to prevent premature release of drug cargo, hyperbranched poly(ethylene imine), PEI, the surface polymer was used as a 'molecular gate' [33] as well as a linker between the MSNs and the targeting ligand MTX (Scheme 2). In summary, our results showed that MTX-conjugated and FTY720-loaded MSNs can be used as carrier systems for targeted drug delivery enabling selective induction of apoptosis, slowing down tumor progression and migration of invasive thyroid cancer cells.

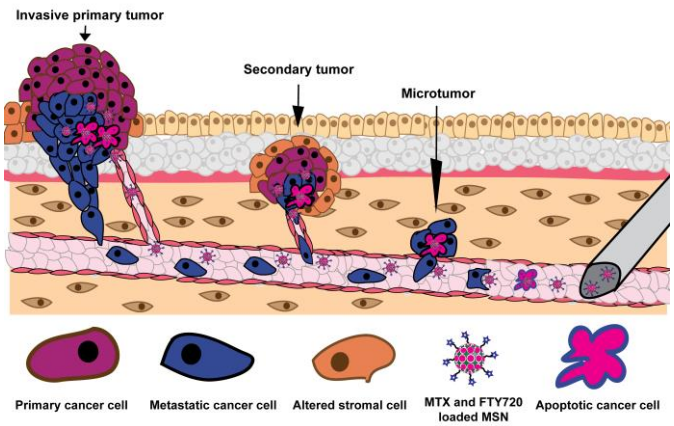

Scheme 1. Schematic representation showing the general principle of the envisioned effect of the MTX surface-functionalized and FTY720 multidrug-loaded nanoparticles on folate receptor-expressing metastatic cancer cells.

Results and discussion

The synthesis and characterization of mesoporous silica nanoparticles

Folic acid (FA) conjugated, poly(ethylene imine), PEI, functionalized mesoporous silica nanoparticles (MSNs) were first synthesized, as folate receptor (FR) mediated targeted drug delivery systems have previously been proven to deliver hydrophobic cargo to FR positive cancer cells with only minimal off-target effects in normal cells [14,22,32,34]. Thereafter, we replaced the folic acid functionalization with methotrexate (MTX) - a folate antagonist that have an anti-cancerous effect as well as targeting ligand capabilities (Scheme 2). Particle size was determined by scanning electron microscopy (SEM), showing particles of uniform size with a diameter of 300 nm, whereas the porous structure of the nanoparticles was elucidated by transmission electron microscopy (TEM; Fig. 1). The PEI weight amount was determined by thermogravimetrical analysis (TGA) and was around 34-weight % (Supp. Fig 1). The PEI functionalization was further confirmed by measuring the change in zeta potential of MSNs from ~8 mV to + 58 mV, and the hydrodynamic diameter of particles was determined by dynamic light scattering (DLS) technique confirming full dispersibility in aqueous solution (Supp. Fig 1). The amount of MTX and FTY720 conjugated onto/loaded into the MSNs was deduced from UV/Vis and found to be 1.99% weight percent (wt %) for the MSN-PEI-MTX_{org} and 2.1 wt% for the MSN-PEI-MTX_{aq}. The conjugation that gave the highest yield was selected for further studies and the FTY720 loading degree was 27.9 wt% in the selected MTX_{aq} particles.

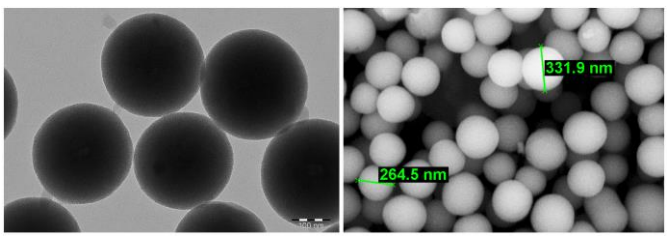

Fig. 1. Electron microscopy images of the synthesized MSNs. Transmission electron microscopy image (TEM; left) revealing the porous structure with radially aligned mesopores; and scanning electron microscopy image (SEM; right) with the ruler in green showing the particle diameters around 300 nm. Scale bar-100 nm (TEM image).

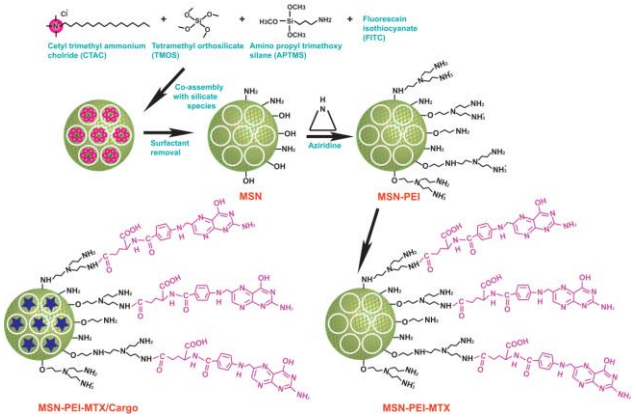

Scheme 2. Schematic representation of the synthesis and functionalization of the designed MSNs.

Cellular uptake of functionalized MSNs in cancerous vs normal thyroid cells by flow cytometry and confocal microscopy

We investigated the uptake rate of FA and MTX conjugated MSNs in two different epithelial thyroid cells lines expressing FR (Fig 2). The selected cell lines were: ML-1 (follicular thyroid carcinoma cells) and Nthy-ori 3-1 (normal human primary thyroid follicular epithelial cells) and the uptake efficacy was determined by flow cytometry and confocal laser scanning microscopy (CLSM) at a concentration of 1.5 µg/ml for 4 hours. The flow cytometry results showed that the MSN-PEI-FA were internalized at a significantly higher level in the cancerous thyroid cells as compared to the normal thyroid cells (Fig. 2c). This difference in uptake efficacy could be explained by the difference in FR expression between the normal and cancerous thyroid cells seen in the western blot results (Fig. 2a&b). To confirm the intracellular localization as well as the enhanced affinity towards cancerous cells, the cell membrane was stained with rhodamine-lectin and imaged by CLSM to determine whether the particles were inside or outside the cell membrane. The confocal images verified that these FA conjugated nanoparticles were internalized in higher quantities by ML-1 cells than by Nthy-ori 3-1 cells, and that the fluorescence from the FITC channel originated from nanoparticles localized inside the cell membrane confirming particle internalization (Fig. 2d&e).

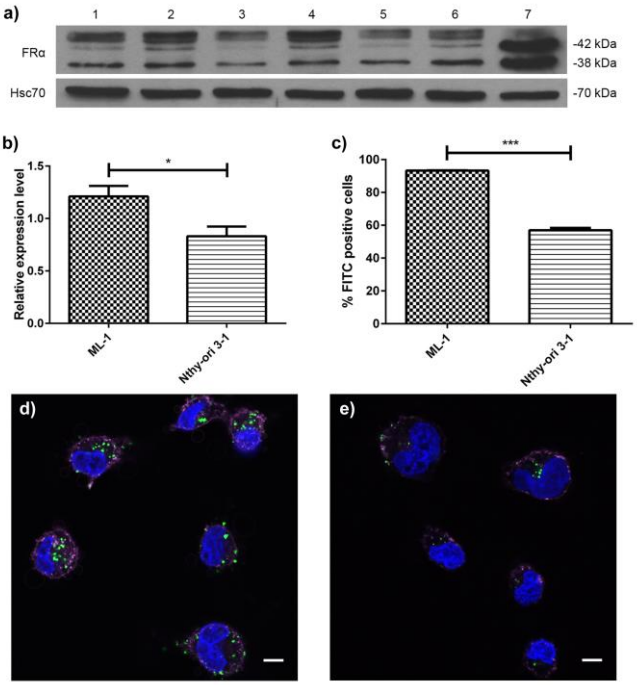

Fig. 2. Folic acid conjugated nanoparticle internalized more efficiently in the cancerous thyroid cells compared to the normal thyroid cells. a) FR protein expression in Nthy-ori 3-1 cells (1,3,5), ML-1 cells (2,4,6), and HeLa cells (7) as a FRα positive control. b) Quantification of FRα protein levels in Nthy-ori 3-1 cells and ML-1 cells. c) Flow cytometry quantification of cellular uptake of MSNs shown as % FITC positive cells using 1.5 µg/ml of nanoparticles in ML-1 cell compared to Nthy-ori 3-1 cells after 4 hours incubation. Confocal microscopy images of MSN-PEI-FR endocytosis in d) ML-1 cells and e) Nthy-ori 3-1 at 1.5 µg/ml for 4 hours with scale bar of 10µm. Error bars represent ± SEM (n≥3). *, $P \leq 0.05$, ***, $P \leq 0.001$.

When investigating the effect of surface functionalization between PEI and MTX conjugated particles on the internalization efficacy in the selected cell lines, the results show that the MSN-PEI-MTX provided higher cellular uptake compared to that of MSN-PEI (Fig. 3). Statistical analysis revealed that the MSN-PEI-MTX yielded significantly higher particle uptake in both the normal (Nthy-ori 3-1) and the cancerous thyroid (ML-1) cells compared to MSN-PEI demonstrating MTX as a potential active targeting ligand (Fig. 3). Intriguingly, differences in the particle uptake of the two targeting ligands, FA and MTX, could be a result of the drug MTX already starting to affect cell homeostasis pushing the cells towards apoptosis, thus lowering particle internalization in the MSN-PEI-MTX compared to the MSN-PEI-FA (Fig. 2&3). Another possible explanation could be due to the targeting ligand MTX having slightly lower affinity for the FR than FA and would therefore be less efficiently internalized by FR expressing cells [35,36]. Even though there are particles being internalized in the normal thyroid cells, this would not pose any major concern as normal adult post-mitotic cells, in this case thyroid cells, do not actively divide and would thus not be effected in the same extent than fast dividing cancer cells by the anti-cancerous effect of MTX [26,27,37,38].

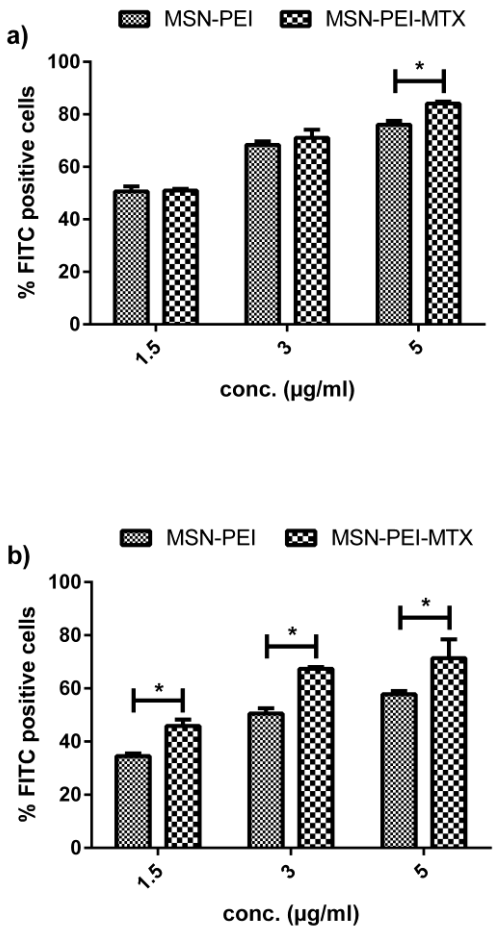

Fig. 3. Flow cytometry quantification of the cellular uptake of PEI and MTX functionalized MSN using 1.5, 3 and 5 µg/ml of nanoparticles in cancerous thyroid cells and normal thyroid cells after 4 hours of incubation. a) % FITC positive ML-1 cells show highest internalization of the MSN-PEI-MTX at 5 µg/ml. b) % FITC positive Nthy-ori 3-1 cells gives lower overall internalization of functionalized nanoarticles than the cancerous counterparts. Error bars represent ± SEM (n=3). *, $P \leq 0.05$.

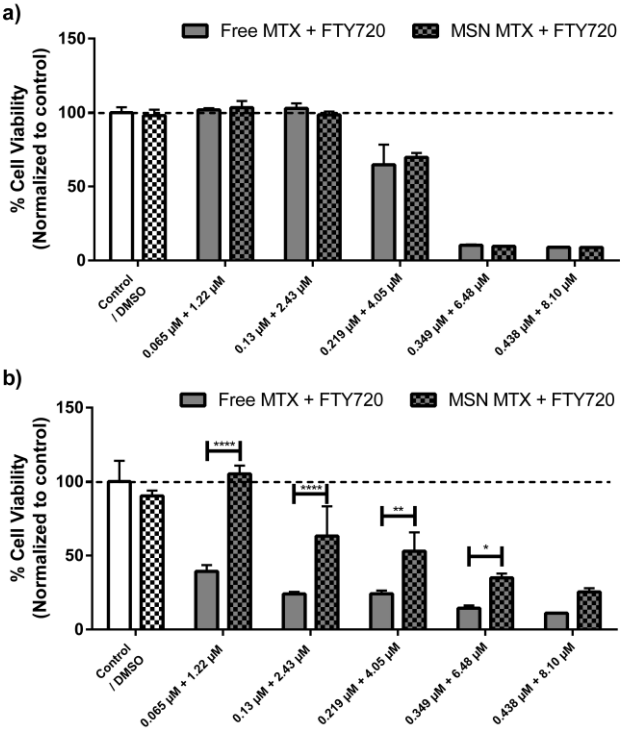

Fig. 4. Viability measurement using the WST-1 metabolic assay for detecting the different treatments efficacy in cancerous thyroid cells and normal thyroid cells after 72 hours of incubation. a) The cell viability decreases when the drug concentration increases in the ML-1 cells in using both the free drug combination and the drug-loaded MSNs. b) The Nthy-ori 3-1 cells are sensitive to the free drug cocktail whereas the drug-loaded MSN shows significantly less off-target effects. Increasing drug concentrations of MTX and FTY720 were used and the viability values were normalized to control (untreated sample) next to 0.2% weight by volume (w/v) DMSO (vehicle control). Error bars represent ± SEM (n=3). *, $P \leq 0.05$, **, $P \leq 0.01$, ****, $P \leq 0.0001$.

Cytotoxicity of MTX and FTY720-loaded nanoparticles

We analyzed the metabolic activity as a viability measurement of both thyroid cell lines treated with FTY720 loaded in the selected carrier system (MSN-PEI-MTX) compared to free drug cocktail. The ML-1 cells treated for 72h with either free drug combination or drug-loaded MSNs showed both a concentration-dependent decrease in cell viability (Fig. 4a). More importantly, the drug-loaded MSNs had significantly less toxicity in the normal thyroid cells compared to the free drug-treated samples (Fig. 4b). Based on the viability measurements, the optimal dose resulting in decreased metabolic activity in the cancerous ML-1 cells without inducing any major toxicity in the normal Nthy-ori 3-1 cells was around 0.219 µM MTX and 4.05 µM FTY720 (Fig. 4). This concentrations and incubation time were selected for further testing of the anti-cancerous efficacy of the drug combination.

The cytotoxicity assay showed that the multidrug-loaded MSN had lower off-target effects in the normal thyroid cells in terms of apoptosis compared to free drug and that the drug-loaded MSN had higher efficacy in ML-1 cells than free drug (Fig. 5). Additionally, the drug-loaded MSNs showed an enhanced anti-cancerous effect and lower cytotoxicity in normal cells validated by cell counting and crystal violet staining (Supp. Fig. 2).

In order to rule out that the effect was not due to the particles themselves, "empty" MSNs (without MTX and FTY720) were administered to both cell lines. The result shows that no significant toxicity was detectable when using similar particle concentrations as in our drug-loaded MSNs experiment (1.5 – 12 µg/ml). However, when treated high concentrations of non-loaded particles (60 µg/ml) the cell viability of normal Nthy-ori 3-1 cells was significantly decreased whereas no significant change was detected in the cancerous ML-1 cells (Supp. Fig. 3). This difference in viability after administration of "empty" MSNs could be a consequence of cancerous cells having a different metabolic activity then normal cells affecting the outcome of the treatment [39–42]. Taken together, the *in vitro* viability measurements demonstrates an enhancement in drug efficacy when loading the drug combination in the designed MSNs compered to free drug treatment.

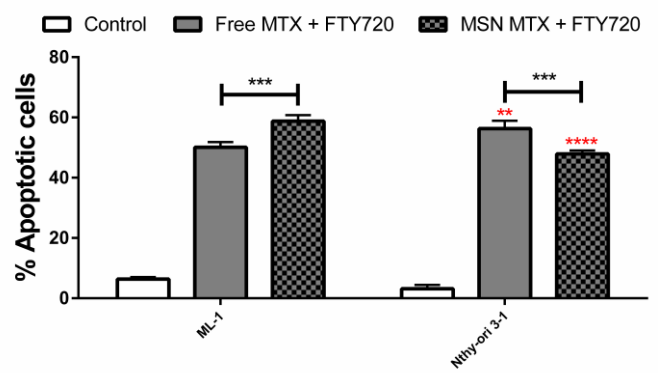

Fig. 5. Flow cytometry toxicity measurement of free drug cocktail of MTX and FTY720 or MSN loaded with MTX and FTY720 in normal versus cancerous thyroid cells. The free drug shows significantly higher toxicity in the normal thyroid (Nthy-ori 3-1) cells compared to the cancerous (ML-1) cells and the drug-loaded MSN shows higher efficacy in the cancerous thyroid cells compared to free drug as well as lower off-target effect in the normal thyroid cells. Statistics in black indicate comparison between free drugs versus drug-loaded MSN. Concentration used was 0.219 µM MTX and 4.05 µM FTY720. Statistical significance between ML-1 versus Nthy-ori 3-1 cells indicated by red asterisks. Error bars represents ±SEM (n=3). **, $P \leq 0.01$, ***, $P \leq 0.001$, ****, $P \leq 0.0001$.

Label free imaging techniques validates targeted drug delivery

In order to validate the enhanced drug efficacy by MTX conjugated and FTY720 loaded MSNs, we utilized image analysis performed by external experts using label-free imaging instrumentation VL21 (Phasefocus Ltd, Sheffield, UK) [43]. The acquired images showed that ML-1 cells treated either with free drug cocktail or the drug-loaded MSNs at concentrations of 0.219 µM MTX and 4.05 µM FTY720 both showed a rounded up phenotype, whereas control sample cells were elongated and spread out (Fig. 6a). Additionally, the image analysis of the cells treated with the drug cocktail displayed a significant reduction in volume compared to control cells after 4 days of treatment (Fig. 6b). Indeed, blebbing, which is evident in VL21 images of both drug-treated groups from day 3 onwards, is often accompanied (and followed by) a reduction in cell volume as cells die [44].

Furthermore, the statistical analysis performed on the quantified image data verifies that both free drug and drug-loaded MSNs decreases cell volume after 72 hours of incubation, compared to control, and that sphericity was significantly decreased in the multidrug-loaded MSNs compared to the free drug combination treatment (Fig. 6b&c). The quantification together with the reconstructed VL21 images shows that these ML-1 cells exhibit a more apoptotic/necrotic phenotype seen as blebbing of cells after administration of FTY720- and MTX-loaded nanoparticles compared to cells administered the drug cocktail (Fig. 6).

Taken together, promising *in vitro* results were obtained regarding the potential of this particle system's selectivity towards folate receptor-expressing cancer cells. The *in vitro* results demonstrates that our proposed multidrug-loaded MSN could potentially be considered to combat cancer cells originated from the thyroid gland. As the poorly water-soluble drugs, MTX and FTY720, anti-cancerous efficacy was significantly enhanced compared to free drug while keeping the off-target effect on normal thyroid cells minimal.

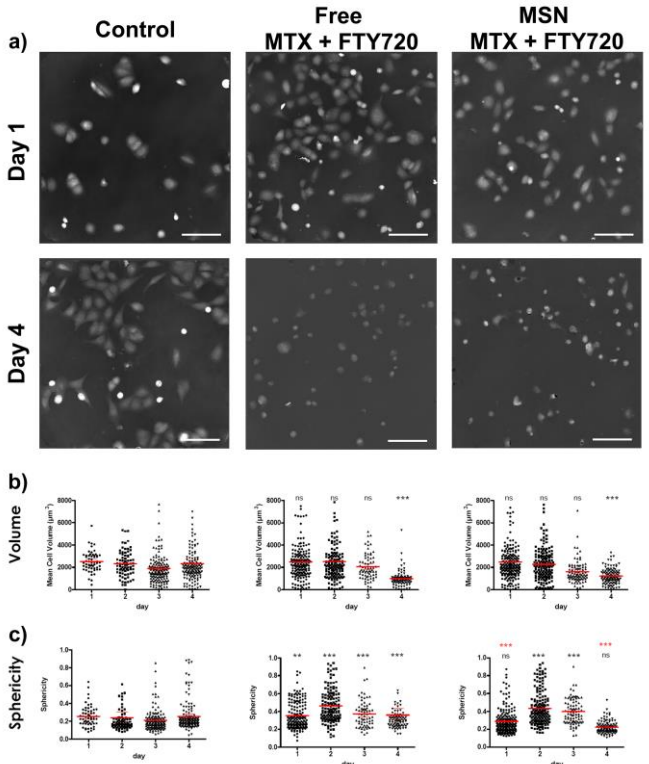

Fig. 6. Phasefocus measurements of ML-1 cancer cells treated with MTX and FTY720 or MSN loaded with a combination of these drugs. a) The multidrug-loaded MSN treated cells showed a more condensed and rounded up phenotype than the free drug-treated cells after 4 days of incubation, scale bar 150 µm. Image quantification showing the b) volume and c) sphericity of the cell populations in control, free drug, and drug-loaded MSN. The image analysis shows that the ML-1 cells administered with drug-loaded MSNs after 4 days of incubation have a less spherical phenotype and are smaller in volume compared to cells treated with free drugs. Statistics in black indicate comparison between control and drug-treated samples. Points of statistical significance between control and treated samples or difference between free drug samples and drug-loaded MSNs indicated by red asterisks. Drug concentration used was 0.219 µM MTX and 4.05 µM FTY720. Number of cells analyzed (n=1524). Error bars represent ± SEM. **, $P \leq 0.01$, ***, $P \leq 0.001$.

In vitro invasion assay validates the invasive behavior of ML-1 cells and the potential inhibitory effect of the drug cocktail

In order to see if the drug cocktail affects the invasion of ML-1 cells we have used the Boyden chamber invasion assay [45,46]. The ML-1 cells exhibited very high invasion properties, thus the optimal time for the assay was set at 7 hours (data not shown). The concentration of MTX and FTY720 were as follows: the low dosage was 0.13 µM MTX and 2.43 µM FTY720, and the high dosage was 0.438 µM MTX and 8.10 µM FTY720. The result shows that the high drug dosage (0.438 µM MTX and 8.10 µM FTY720) efficiently inhibits the invasion of the ML-1 cells (Fig. 7). This suggests the potential use of the drug combination in blocking invasiveness and thus the metastatic potential of thyroid cancer cells.

Intriguingly, the lower dosage significantly increases the cancer cell invasion functioning as an accelerant. This was seen as an increased migration of the ML-1 cells from the upper well towards the lower well (Fig. 7). However, such opposite effect of the low concentrations drug cocktail would need further study in order to validate the underlying mechanism seen in this study. Nevertheless, several other studies have shown that a drug can exhibit a biphasic effect, where the low dosage has a stimulating effect, and the high dose has an inhibitory effect [47].

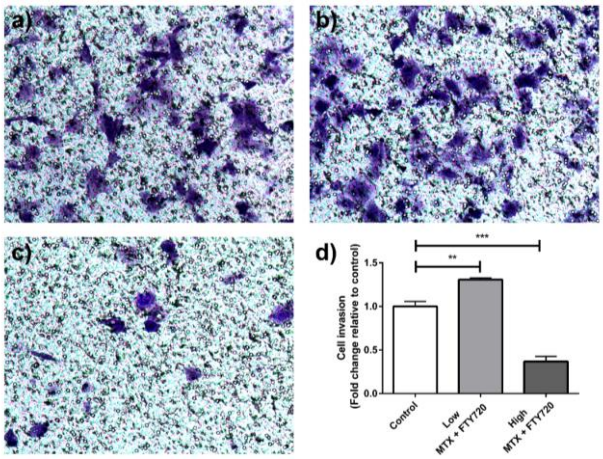

Fig. 7. Invasion assay showing crystal violet-stained ML-1 cells after 7 hours. a) In the control sample, ML-1 cells are visible on the insert after 7 hours showing that the cells are highly invasive. b) Low dosage of combination treatment (0.13 µM MTX and 2.43 µM FTY720) shows slight increase in the invasive potential of the ML-1 cells compared to control. c) The high dosage (0.438 µM MTX and 8.10 µM FTY720) show less migrating ML-1 cells on the insert and the d) quantification of the invasion assay validates that the high combination treatment block the invasiveness of these ML-1 cells. Error bars represent ± SEM (n=4). **, P ≤ 0.01, ***, P ≤ 0.001.

In vivo drug efficacy studies utilizing Chick chorioallantoic membrane assay

To determine the enhanced anti-migratory and anti-cancerous efficacy of our multidrug-loaded nanoparticles *in vivo* we utilized ML-1 derived tumors grown on the Chick chorioallantoic membrane (CAM) by measuring tumor weight and estimating tumor size by image quantification combined with histology for classifying tumor phenotypes [48–51]. The *in vivo* result shows that the untreated xenografts (administered 0.5% DMSO as control or 1.6 mg/ml of empty MSN) had a significant reduction in tumor size and weight from pre-treatment to post-treatment as a consequence of the invasive nature of these ML-1 cells (Fig. 8) [29,52].

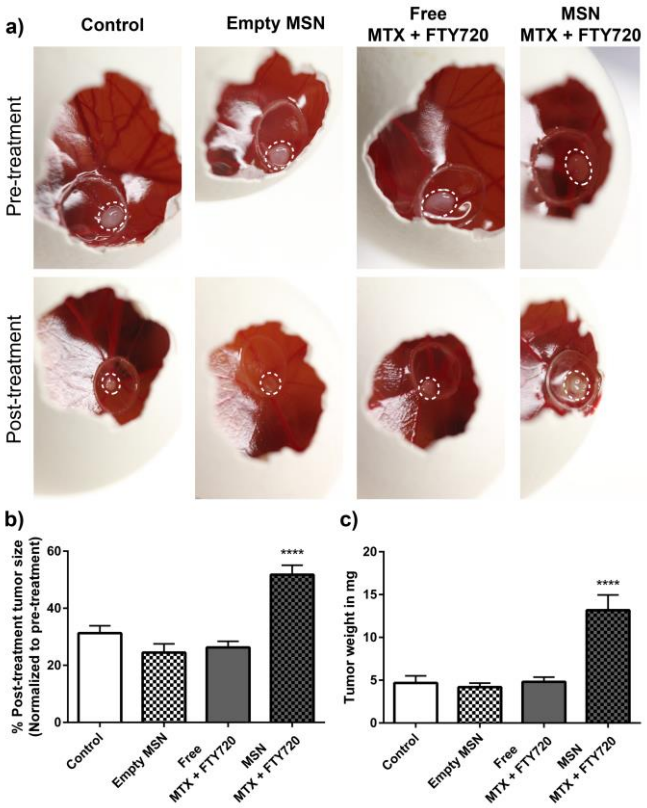

Fig. 8. Chick chorioallantoic membrane (CAM) assay for evaluating the *in vivo* drug efficacy in terms of inhibiting invasion of ML-1 derived tumors. a) Representative images of xenografts indicated by white dotted circles before and after treatment showing tumor phenotype in control (0.5% DMSO), particle control (1.6 mg/ml empty MSN) and free drug treatment (1 µg MTX and 13 µg FTY720). The drug-loaded MSNs (1 µg MTX and 13 µg FTY720) treatment showed clear retention in post-treatment tumor size as well as yellow and white discolorations as signs of inflammation and necrosis. b) Image quantification of mean visible tumor size of post-treated tumors normalized to pre-treated tumors size shows decreased tumor size on all samples except the drug-loaded MSN showing retention of tumor size c) Post tumor weighing (in mg) shows significantly larger tumors after the drug-loaded MSN treatment. Error bars represent ± SEM (n≥4). **** P ≤ 0.0001.

The hematoxylin and eosin (H&E) staining of whole tumors validated the invasive phenotype observed *in vivo*. This was seen in the non-drug treated samples as the ML-1 cells were migrating into the CAM suggesting that the cancer cells 'escaped' the xenograft and invaded the underlying mesoderm, thus reducing the tumor size and weight (Supp. Fig 4). After 3 consecutive days of drug administration, both the free drug and drug-loaded MSN showed significant retention of tumor size on the CAM as compared to the tumors administered free drug cocktail or control tumors (Fig. 8b&c). Additionally, we detected a necrotic phenotype of the tumors that were administered the drug-loaded MSNs. This was visually detectable in the images seen as disrupted tumor morphology and discoloration of the tumor mass (Fig. 8a) [53]. Indicating that the multidrug-loaded MSNs have an enhanced ability to induce apoptosis/necrosis in ML-1 derived tumors grown on the CAM compared tumors treated with the free drug.

Furthermore, tissue analysis using hematoxylin-eosin (H&E) staining showed a higher dispersion of cells in control and empty particle samples whereas the drug-treated cells seem more aggregated and condensed (Fig. 9). The untreated ML-1 xenografts expressed higher thyroid transcription factor 1 (TTF1) than both drug-treated samples indicating invasive tumor phenotype of these thyroid derived cancer cells [54]. Also, the xenografts had some basal cleaved caspase-3 activity in all samples (Fig. 9). However, increased cleaved capsase-3 activity has been shown to be elevated in metastatic thyroid carcinomas compared to normal thyroid tissue [55]. Tumors treatment with the drug-loaded MSN showed lower expression of the epithelial-mesenchymal transition (EMT) marker vimentin (VIM), indicating lower invasiveness and metastatic potential of these ML-1 xenografts [56]. The H&E staining of the drug-loaded MSNs treated tumors showed an increased nuclear condensation and cell fragmentation indicating a more necrotic phenotype compared to the tumors administered with the free drug cocktail (Fig. 8) [44].

Taken together, our *in vivo* results showed that MTX and FTY720 loaded MSNs have an advantage in terms of anti-cancerous activity and inhibition of the invasive phenotype of these ML-1 dervided xenografts compared to that of the freely administered drug cocktail. Taking into account the significant adverse effects related to chemotherapy used for metastatic tumors, including aggressive tumors originated from the thyroid gland, the use of multidrug-loaded MSNs could clearly be an option worth developing further.

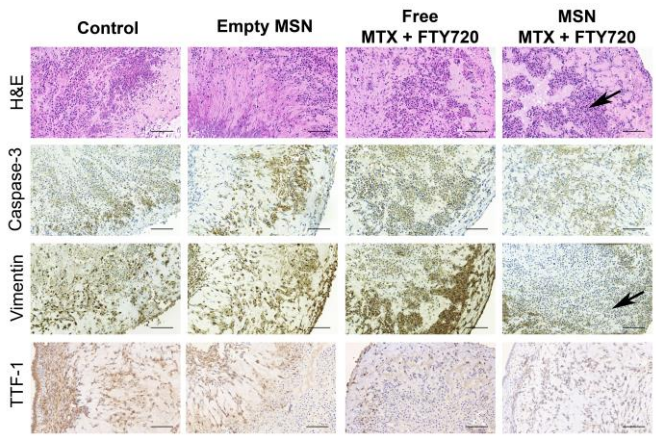

Fig. 9. Representative images of ML-1 xenografts grown on CAM stained by hematoxylin-eosin (H&E), thyroid cancer marker (TTF1), cleaved caspase3 and vimentin staining. The black arrow in the H&E staining shows necrotic areas induced by drug-loaded MSNs. The black arrow in the vimentin staining shows less active epithelial-mesenchymal transition (EMT) in the ML-1 derived tumors after drug-loaded MSNs treatment. Scale bar 50 µm.

Materials and methods

Synthesis and modification of mesoporous silica nanoparticles

A particle system comprising of a MSN core and PEI coating with or without FA was synthesized according to our previously published protocols [14,57,58]. For the modification of MTX-functionalized MSNs, two different conjugation protocols were used. In the first protocol, the MSN-PEI-MTX_{aq} was synthetized by dissolving a 100 µg portion of MTX in ethanol, to which 5 µL of EDC (1-ethyl-3-(3-dimethylaminopropyl)carbodiimide) crosslinker was added to react with the carboxyl groups of MTX. To increase the yield of EDC-mediated amine coupling, 250 µL of a 1 mg/mL NHS-solution (N-hydroxysuccinimide) was added and kept stirring for one hour at room temperature (RT). This solution was then mixed with the particle suspension (50 mg in MES buffer; 10 mM, pH 5.5) and was agitated for 4 hours at RT. Afterwards, the particles were centrifuged, washed and vacuum dried to yield MSN-PEI-MTX_{aq}. To obtain MSN-PEI-MTX_{org}, a 100 µg portion of MTX was dissolved in dimethyl formamide (DMF), to which 250 µL of HATU solution ((O-(7-azabenzotriazol-1-yl)-N,N,N,N0-tetramethyl-uronium-hexafluoro-phosphate) 1 mg/ml in DMF) was added to activate the carboxylic acid groups of MTX. This solution was then mixed with the particle suspension 50 mg/ mL in DMF and was agitated for 4 hours at RT. Afterward, the particles were centrifuged, washed and vacuum dried to yield MSN-PEI-MTX_{org}. To load FTY720 (Sigma-Aldrich, St. Louis, MO, USA) into the pores of the mesoporous silica particles, the particles were dispersed in cyclohexane to which desired amounts of a solution of FTY720 in cyclohexane were added. The resultant loading suspension was stirred for 24 hours, followed by centrifugation and washing extensively with cyclohexane to remove any loosely adsorbed FTY720, obtaining the drug-loaded MSNs. Scanning and transmission electron microscopy were used to confirm the size, monodispersity, morphology and non-agglomerated state of the particles. To find out the amount of drug loading in the MSNs, samples will be dispersed in ethanol for complete drug elution. The concentration of the drug was determined by UV/vis spectroscopy measurements at a wavelength of 425 nm and from that measurement, the drug loading amount can be calculated.

Cell culture

Thyroid follicular cancer cells (ML-1) provided by Dr. Johan Schönberger (University of Regensburg, Germany) and human cervical carcinoma (HeLa) cells obtained from ATCC (Manassas, VA, USA) were maintained in DMEM medium (Sigma-Aldrich, St. Louis, MO, USA) supplemented with 10% fetal bovine serum (FBS; BioClear, Wiltshire, UK), 2 mM L-glutamine, 100 U/ml penicillin, 100 µg/ml streptomycin at 37°C in a 5% CO2/95%O2 and 90% RH humidify atmosphere and handled under sterile conditions. Normal thyroid cells (Nthy-ori 3-1; Culture Collections, Public Health England, Porton Down, Salisbury, UK) were cultured in RPMI 1640 (Sigma-Aldrich) with 2mM L-glutamine, 10% FBS, 100 U/ml penicillin and 100 µg/ml streptomycin in similar culture conditions.

Cellular uptake of MSNS by flow cytometry and confocal microscopy

MSNs were suspended in cell medium at 1.5 µg/ml, sonicated for 30 min, then applied on 50-70 % confluent cells and incubated for 4 hours at 37°C. The extracellular fluorescence was quenched by resuspension in 200 µg/ml trypan blue (Sigma-Aldrich) for 10 minutes at room temperature. The amount of endocytosed particles inside cells was analyzed by BD FACSCalibur flow cytometer (FL-I, BD Pharmingen). The data was analyzed using BD CellQuest Pro™ software for calculating the amount in percentages of MSNs uptake by 10 000 cells.

For microscopical studies, cells grown on sterile coverslips were incubated with 1.5 µg/ml particles for 4 hours. After incubation the extracellular fluorescence were quenched with trypan blue (200 µg/ml) for 10 minutes at room temperature. Then the cell were washed two times with PBS and labeled with rhodamine-lectin (Vector Laboratories, Burlingame, CA, USA) for 15 minutes at 37 °C then fixed with 3.7% paraformaldehyde containing 0.5% Triton X-100 for 15 minutes at room temperature. Coverslips with cells were mounted on slides in VECTASHIELD® Mounting Media containing DAPI (Vector Laboratories) and particle uptake was analyzed using a Zeiss LSM510 META confocal microscope with 63x oil objective. Using 488 nm excitation and 500-550 nm emission for detecting the FITC channel and 405 nm excitation with 420-480 nm emission for detecting the DAPI channel as well as an excitation of 543 nm and an emission of 570-600 nm for detecting the rhodamine-lectin channel.

Western blot analysis

Western blot analysis was utilized in order to estimate the folate receptor expression levels in ML-1 and Nthy-ori 3-1 cells. Whole-cell extracts were lysed with Laemmli buffer containing β-mercaptoethanol and the proteins were denaturated at 95 °C for 10 minutes. Proteins were separated by 10% SDS-PAGE and transferred to nitrocellulose membranes. Folate receptor alpha antibody (FOLR1; Lifespan Biosciences Inc., Seattle, WA, USA) was used at 1:1000 dilution and anti-Hsc70 (StressGen Biotechnologies Corp., Victoria, Canada) was used at 1:10000 dilution. Horseradish peroxidase-conjugated secondary antibodies (GE healthcare, Buckinghamshire, UK) were detected using enhanced chemiluminescence kit (Amersham Biosciences Corp., Piscataway, NJ, USA). Densitometric analysis of the FOLR1 staining was performed using imageJ and normalized to the loading control (Hsc70) [59].

***In vitro* cytotoxicity assay**

ML-1 and Nthy-ori 3-1 cells were seeded on separate 96-well plates and allowed to attach overnight. After 24 hours, the medium was removed and replaced with 100 µL medium containing different concentrations of MSNs (1.5, 3, 5, 8, 10 µg/mL) equivalent to 0.065 µM, 0.13 µM, 0.219 µM, 0.349 µM, 0.438 µM free MTX and 1.22 µM, 2.43 µM, 4.05 µM, 6.48 µM, 8.10 µM free FTY720 and incubated for 72 hours. After the incubation period, 5 µL of WST-1 reagent (Roche Applied Science, Upper Bavaria, Germany) was added to each well and the plate was further incubated for 90 minutes at 37 °C. The absorbance of the colored formazan was measured at 430 nm using the Varioskan microplate reader (Thermo Scientific, Logan UT, USA).

Cytotoxicity measurement by flow cytometry

DNA starts to fragment in apoptotic cells that can be measured by flow cytometry when using propidium iodide (PI) staining which binds to the fragmented DNA allowing selective detection of the apoptotic population [60]. The ML-1 and Nthy-ori 3-1 cells were seeded in a 12-well culture plate and incubated with either free MTX and FTY720 or MSN loaded with MTX and FTY720 at 0.438 µM MTX and 8.10 µM FTY720 concentrations. After 72 hours incubation, the cell medium was collected and the cells were washed and harvested using trypsin-EDTA suspension for 5 minutes at 37 °C. Samples were centrifuged for 5 minutes, washed with PBS and re-suspended in 400 µl of lysis buffer (0.3% Triton X-100, 0.05 mg/ml PI, 40mM sodium citrate and 1 mg/ml RNase A) for 10 minutes at 37 °C to obtain the nuclear fraction of the cells. The samples were immediately analyzed by a BD FACSCalibur flow cytometer (FL-3, BD Pharmingen, San Diego, California, USA) at 488 nm excitation and 670 nm emission with 10000 cells analyzed per sample. The percentage of apoptotic cells defined as sub-G1 phase was analyzed using BD CellQuest Pro™ software (BD Pharmingen, San Diego, CA, United States).

Cell morphology detected by label-free imaging technique

ML-1 thyroid cancer cells were grown on sterile 6-well plate and on the next day the drug cocktail or drug-loaded MSN were administered using 0.219 µM MTX and 4.05 µM FTY720 concentrations. The samples were imaged using the VL21 instrument (Phasefocus Ltd, Sheffield, UK) with 20x magnification using 20 minutes intervals per region of interest (ROI) for a duration of 72 hours. The technique uses light for reconstructing an image of the samples refractive properties without labeling and toxic lasers [43]. The aim of the investigation was to identify apoptotic phenotypes in the ML-1 cells administered either free drug cocktail or drug-loaded MSNs using label-free image analysis performed by experts from Phasefocus Ltd.

Boyden invasion assay

Boyden chamber invasion experiments were conducted with Transwell Permeable Support inserts with 6.5 mm diameter and 8 µm pore size (Corning Inc; Corning, NY, USA) and the inserts were coated with 5.0 µg/cm^2 human collagen IV (Corning). Then 100 000 cells were added into the upper well that contained 10% FBS cell medium and in the lower well, 20% FBS was added as a chemoattractant. The concentration of MTX and FTY720 were as follows: the low dosage was 0.13 µM MTX and 2.43 µM FTY720, the high dosage was 0.438 µM MTX and 8.10 µM FTY720 and the test substances were present in both wells. Cells were allowed to invade for 7 hours. Cells from the upper well

cells were removed with a cotton swab and the transwell insert was fixed with 2% paraformaldehyde solution in PBS for 10 minutes and stained with 0.1% crystal violet solution in 20% methanol for 5 minutes. The inserts were then washed twice with PBS and once with Milli-Q water and allowed to dry overnight. Cells were counted with 40x magnification from eight microscopic fields per insert.

In vivo drug efficacy studies

Fertilized chicken eggs from White Leghorn chickens (LSK Poultry Oy, Laitila, Finland) were sterilized by wiping with 70% ethanol, placed into rotation racks and incubated on rotation mode at 37°C and 40-50% relative humidity for three days. On embryonal developmental day (EDD) 3, a 3mm^2 hole was made on the apical side of the eggs, allowing the formation of an air pocket between the chorioallantoic membrane and the eggshell. The holes were sealed using scotch tape and the eggs were returned to the incubator. The holes were enlarged on EDD 8; thereafter one sterile silicone ring was placed atop a prominent superficial blood vessel in every egg. For each egg, one million of ML-1 thyroid cancer cells suspended in 10 µl of phosphate-buffered saline was mixed 1:1 with Matrigel (Corning, Growth Factor Reduced Basement Membrane Matrix (REF:356231) and seeded onto the CAM. The eggs were sealed with laboratory plastic film and the tumors were allowed to develop overnight. The tumors were photographed on the next day (EDD 9); thereafter the xenografts were topically treated once a day for three consecutive days. Stock solutions of drug cocktail (MTX and FTY720) were prepared by dissolving in DMSO to the concentrations 6.7 mg/ml and 67 mg/ml, to ensure that the final concentration of DMSO would not exceed 0.5% (w/v) per egg treatment.

During the drug efficacy testing the stock solutions in DMSO were diluted in HEPES to concentrations ranging from 1-10 µg of FTY720 / 30 µl (33.3-333.3 µg/ml) and 0.1-1 µg MTX / 30 µl (3.3-33.3 µg/ml) and the treatment volume was 30 µl per egg. When comparing the treatment efficacy between combined free drugs and nanoparticle-loaded drugs, eggs were treated with 0.1 µg MTX and 1.3 µg FTY or 1 µg MTX and 13 µg FTY (equal to 160 µg/ml and 1.6 mg/ml nanoparticles, respectively). Controls were treated with 0.5% DMSO in HEPES or equal amounts of empty nanoparticles in HEPES in experiments with nanoparticle treatments. The tumors were photographed on EDD 9 and EDD 12 in order to obtain visual observation of pre- and post-treated tumors. Image quantification were then performed on the images using ImageJ by manually selecting the tumor area of first the pre-treated tumors then comparing that area with the post-treated tumor area of the same tumors giving the difference in tumor size in percentages [29]. The tumors were then excised and weighed as an endpoint measurement in order to verify tumor weight (in mg) on EDD 12 [48]. Tumors were then fixed in 3 % paraformaldehyde solution in PBS (PFA) and dehydrated in a rising ethanol series prior to paraffin embedding, for further sectioning and histological staining.

Immunohistochemistry

Paraffin-embedded tumors grown on CAM from all experimental groups (n=4/ group) were cut into 4±1 µm sections and immunohistochemically stained with antibodies and reagents listed in supplementary Table 1. In brief, antigens were retrieved using high-temperature in Tris-EDTA buffer (pH9), washed in TBS with 0.1% Tween20 (TBST; #P1379, Sigma-Aldrich, Saint Louis, MO), blocked in 3% bovine serum albumin (BSA; #A9418, Sigma-Aldrich) in TBST for 1 hour at RT, incubated overnight with the primary antibody. Next day slides were washed 3x with TBST, incubated with secondary antibody for 30 min, washed 3x in TBST and visualized using Liquid DAB+ Substrate Chromogen System (Dako, Glostrup, Denmark). Slides were scanned by Pannoramic 250 Slide Scanner (3DHISTECH Ltd., Budapest, Hungary) and images were taken using CaseViewer (3DHISTECH).

Statistical analysis

Statistical significance (P-value) was determined by One-way or Two-way analysis of variance, Student's t-test, Kruskal-Wallis test with Dunn's post hoc test or Sidak's multiple comparisons test (GraphPad Prism® 6.0, San Diego, CA, USA). The Error bars represent plus-minus the standard error of the mean (±SEM).

Conclusions

We investigated the potential use of the folate antagonist methotrexate (MTX) as an active targeting ligand conjugated onto mesoporous silica nanoparticles (MSN) [61] enabling effective particle internalization in folate receptor-expressing thyroid cancer cells. The active ligand MTX has been used in chemotherapy for decades, whereas the anti-cancerous efficacy depends on blocking the synthesis of thymine and purine nucleotides. This, in turn, leads to replication errors pushing fast-dividing cancer cells towards apoptosis [26,27]. We conjugated MTX on the surface of the nanoparticles enabling the addition of the second drug fingolimod (FTY720). This drug FTY720 is a sphingosine kinase 1 inhibitor, blocking the production of sphingosine 1-phosphate (S1P) and consequently, immobilizes invasive cancer cells [28–30]. First, we validated the internalization of folic acid (FA) functionalized MSNs in cancerous thyroid cells compared to normal thyroid cells. Then, we evaluated the uptake efficacy in folate receptor (FR) expressing thyroid cells by two different MTX functionalization approaches; from which the one that had the highest uptake into the thyroid cells was selected for further studies. The chosen design (MSN-PEI-MTX$_{aq}$) was then loaded with the selected drug (FTY720) enhancing the apoptotic efficacy compared to the free drug cocktail while maintaining lower off-target effects. The enhanced drug efficacy of the MSNs was validated by viability measurements and label-free microscopy technique, demonstrating efficient induction of apoptosis in target thyroid cancer cells compared to freely administered drug cocktail. Furthermore, by using the chick chorioallantoic membrane

(CAM) assay [62,63] it was possible to demonstrate *in vivo* that the drug-loaded MSNs efficiently blocked the invasion of thyroid cancer cells towards the underlying mesoderm in the CAM. This was detected by retention of both tumor size and mass on the chorioallantoic membrane combined with histology showing lower metastatic potential and a more necrotic phenotype in the drug-loaded MSNs treated tumors. Taken together, our results suggest that our multidrug-loaded MSNs enables targeted induction of cell death and immobilization of invasive thyroid cancer cells, and could thus be developed for metastatic cancer treatment when conventional drug cocktail treatment could evoke serious negative off-target effects in the patient.

Acknowledgments

The Cell Imaging Core (CIC) at Turku Center for Biotechnology, Pasi Kankaanpää, Jouko Sandholm, and Markku Saari are thanked for technical support and advice. The Laboratory of Electron Microscopy, University of Turku, and the assistance by Markus Peurla during the TEM characterization are acknowledged, and Top Analytica Ltd. is acknowledged for the SEM usage. The Academy of Finland #309374, Finnish Cultural Foundation, Cancer Society of Finland, Jane and Aatos Erkko Foundation, K. Albin Johanssons Foundation, Paulo Foundation, Otto A. Malm Foundation, Swedish Cultural Foundation, Waldemar von Frenckell foundation, Sigrid Jusélius Foundation, Masonry Foundation, Finnish Cancer Foundations, Åbo Akademi University Endowment, and the Turku Doctoral Network in Molecular Biosciences are greatly acknowledged for the financial support.

Notes and references

Electronic Supplementary Information (ESI) available: [supplementary information includes particle characterization by TGA, N_2-sorption and DLS measurement, viability measurement of "empty" MSNs, propidium idodine staining for estimating apoptotic population and histology of whole tumors.] See DOI:xxxx

[1] A. Wicki, D. Witzigmann, V. Balasubramanian, J. Huwyler, Nanomedicine in cancer therapy: challenges, opportunities, and clinical applications, J Control Release. (2015) 200:138-57. doi: 10.1016/j.jconrel.2014.12.030.

[2] F. Bray, J. Ferlay, I. Soerjomataram, R.L. Siegel, L.A. Torre, A. Jemal, Global cancer statistics 2018: GLOBOCAN estimates of incidence and mortality worldwide for 36 cancers in 185 countries, CA Cancer J Clin. (2018) 68(6):394-424. doi: 10.3322/caac.21492.

[3] Y. Huang, S.P. Cole, T. Cai, Y.U. Cai, Applications of nanoparticle drug delivery systems for the reversal of multidrug resistance in cancer, Oncol Lett. (2016) 12(1):11-15.

[4] M.O. Palumbo, P. Kavan, W.H. Jr Miller, L. Panasci, S. Assouline, N. Johnson, V. Cohen, F. Patenaude, M. Pollak, R.T. Jagoe, G. Batist, Systemic cancer therapy: achievements and challenges that lie ahead, Front Pharmacol. (2013) 4:57. doi: 10.3389/fphar.2013.00057.

[5] V.V. Padma, An overview of targeted cancer therapy, Biomedicine (Taipei). (2015) 5(4):19. doi: 10.7603/s40681-015-0019-4.

[6] M. Riihimäki, H. Thomsen, A. Hemminki, K. Sundquist, K. Hemminki, Comparison of survival of patients with metastases from known versus unknown primaries: survival in metastatic cancer, BMC Cancer. (2013) 13:36. doi: 10.1186/1471-2407-13-36.

[7] R.L. Anderson, T. Balasas, J Callaghan, R.C. Coombes, J. Evans, J.A. Hall, S. Kinrade, D. Jones, P.S. Jones, R. Jones, J.F. Marshall, M.B. Panico, J.A. Shaw, P.S. Steeg, M. Sullivan, W. Tong, A.D. Westwell, J.W. Ritchie; Cancer Research UK and Cancer Therapeutics CRC Australia Metastasis Working Group, A framework for the development of effective anti-metastatic agents, Nat Rev Clin Oncol. (2018) doi: 10.1038/s41571-018-0134-8.

[8] B.J Miller, P. Cram, C.F. Lynch, J.A. Buckwalter, Risk factors for metastatic disease at presentation with osteosarcoma: an analysis of the SEER database. J Bone Joint Surg Am. (2013) 95(13):e89. doi: 10.2106/JBJS.L.01189.

[9] S. Tohme, R.L. Simmons, A. Tsung, Surgery for Cancer: A Trigger for Metastases. Cancer Res. (2017) 77(7):1548-1552. doi: 10.1158/0008-5472.CAN-16-1536.

[10] L.Y. Wan g, F.L. Palmer, I.J. Nixon, D. Thomas, S.G Patel, A.R. Shaha, J.P. Shah, R.M. Tuttle, I. Ganly, Multi-organ distant metastases confer worse disease-specific survival in differentiated thyroid cancer. Thyroid. (2014) 24(11):1594-9. doi: 10.1089/thy.2014.0173.S.

[11] M.E. O'Brien, A. Borthwick, A. Rigg, A. Leary A, L. Assersohn, K. Last, S. Tan, S. Milan, D. Tait, I.E. Smith, Mortality within 30 days of chemotherapy: a clinical governance benchmarking issue for oncology patients. Br J Cancer. (2006) 95(12):1632-6.

[12] O.C. Farokhzad, R. Langer, Impact of nanotechnology on drug delivery. ACS Nano. (2009) 3: 16-20.

[13] L.Y. Ramirez, S.E. Huestis, T.Y. Yap, S. Zyzanski, D. Drotar, E. Kodish, Potential Chemotherapy Side Effects What Do Oncologists Tell Parents? Pediatr Blood Cancer. (2009) 52(4): 497–502. doi: 10.1002/pbc.21835.

[14] J.M. Rosenholm, A. Meinander, E. Peuhu, R. Niemi, J.E. Eriksson, C. Sahlgren, M. Lindén, Targeting of porous hybrid silica nanoparticles to cancer cells, ACS Nano. (2009) 3(1):197-206. doi: 10.1021/nn800781r.

[15] Q. Hu, W. Sun, C. Wang, Z. Gu, Recent advances of cocktail chemotherapy by combination drug delivery systems, Adv Drug Deliv Rev. (2016) 98:19-34. doi: 10.1016/j.addr.2015.10.022.P.

[16] M. Zeisser-Labouèbe, F. Delie, R. Gurny, N. Lange N, Screening of nanoparticulate delivery systems for the photodetection of cancer in a simple and cost-effective model. Nanomedicine (Lond). (2009) 4(2):135-43.

[17] P. Nowak-Sliwinska, T. Segura, M.L. Iruela-Arispe, The chicken chorioallantoic membrane model in biology, medicine and bioengineering. Angiogenesis. (2014) 17(4):779-804. doi: 10.1007/s10456-014-9440-7.

[18] N.A. Lokman, A.S. Elder, C. Ricciardelli, M.K. Oehler, Chick chorioallantoic membrane (CAM) assay as an in vivo model to study the effect of newly identified molecules on ovarian cancer invasion and metastasis. Int J Mol Sci. (2012) 13(8):9959-70. doi: 10.3390/ijms13089959.

[19] A. Zijlstra, R. Mellor, G. Panzarella, R.T. Aimes, J.D. Hooper, N.D. Marchenko, J.P. Quigley, A quantitative analysis of rate-limiting steps in the metastatic cascade using human-specific real-time polymerase chain reaction. Cancer Res. (2002) 62:7083–7092.

[20] K.H. Kain, J.W. Miller, C.R. Jones-Paris, R.T. Thomason, J.D. Lewis, D.M. Bader, J.V. Barnett, A. Zijlstra, The chick embryo as an expanding experimental model for cancer and cardiovascular research. Dev Dyn. (2014) 243(2):216-28. doi: 10.1002/dvdy.24093.

[21] N. Parker, M.J. Turk, E. Westrick, J.D. Lewis, P.S. Low, C.P. Leamon, Folate receptor expression in carcinomas and normal tissues determined by a quantitative radioligand binding assay, Anal Biochem. (2005) 338(2):284-93..

[22] F. Porta, G.E. Lamers, J. Morrhayim, A. Chatzopoulou, M. Schaaf, H. den Dulk, C. Backendorf, J.I. Zink, A. Kros, Folic acid-modified mesoporous silica nanoparticles for cellular and nuclear targeted drug delivery, Adv Healthc Mater. (2013) 2(2):281-6. doi: 10.1002/adhm.201200176.

[23] C.M. Paulos, J.A. Reddy, C.P. Leamon, M.J. Turk, P.S. Low, Ligand binding and kinetics of folate receptor recycling in vivo: impact on receptor-mediated drug delivery, Mol Pharmacol. (2004) 66(6):1406-14.

[24] J. Shen, K.S. Putt, D.W. Visscher, L. Murphy, C. Cohen, S. Singhal, G. Sandusky, Y. Feng, D.S. Dimitrov, P.S. Low, Assessment of folate receptor-β expression in human neoplastic tissues. Oncotarget. (2015) 10;6(16):14700-9.

[25] C.J. Weber, S. Müller, S.A. Safley, K.B. Gordon, P. Amancha, F. Villinger, V.M. Camp, M. Lipowska, J. Sharma, C. Müller, R. Schibli, P.S. Low,C.P. Leamon, R.K. Halkar, Expression of functional folate receptors by human parathyroid cells. Surgery. (2013) 154(6):1385-93; discussion 1393. doi: 10.1016/j.surg.2013.06.045.

[26] F.M. Huennekens, The methotrexate story: a paradigm for development of cancer chemotherapeutic agents, Adv Enzyme Regul. (1994) 34:397-419.

[27] P.T. Wong, S.K. Choi, Mechanisms and implications of dual-acting methotrexate in folate-targeted nanotherapeutic delivery, Int J Mol Sci. (2015) 16(1):1772-90. doi: 10.3390/ijms16011772.

[28] J.R Brocklyn, Regulation of cancer cell migration and invasion by sphingosine-1-phosphate, World J Biol Chem. (2010) 1(10):307-12. doi: 10.4331/wjbc.v1.i10.307.

[29] V. Kalhori, M. Magnusson, M.Y. Asghar, I. Pulli, K. Törnquist, FTY720 (Fingolimod) attenuates basal and sphingosine-1-phosphate-evoked thyroid cancer cell invasion, Endocr Relat Cancer. (2016) 23(5):457-68. doi: 10.1530/ERC-16-0050.

[30] C. Loveridge, F. Tonelli, T. Leclercq, K.G. Lim, J.S. Long, E. Berdyshev, R.J. Tate, V. Natarajan, S.M. Pitson, N.J. Pyne, S. Pyne, The sphingosine kinase 1 inhibitor 2-(p-hydroxyanilino)-4-(p-chlorophenyl)thiazole induces proteasomal degradation of sphingosine kinase 1 in mammalian cells, J Biol Chem. (2010) 285(50):38841-52. doi: 10.1074/jbc.M110.127993.

[31] Q.T. Nguyen, E.J. Lee, M.G. Huang, Y.I. Park, A. Khullar, R.A. Plodkowski, Diagnosis and treatment of patients with thyroid cancer. Am Health Drug Benefits. (2015) 8(1):30-40.

[32] J.M. Rosenholm, C. Sahlgren, M. Lindén, Towards multifunctional, targeted drug delivery systems using mesoporous silica nanoparticles--opportunities & challenges. Nanoscale. (2010) 2(10):1870-83. doi: 10.1039/c0nr00156b.S.D.

[33] E. Niemelä, D. Desai, Y. Nkizinkiko, J.E. Eriksson, J.M. Rosenholm, Sugar-decorated mesoporous silica nanoparticles as delivery vehicles for the poorly soluble drug celastrol enables targeted induction of apoptosis in cancer cells. Eur J Pharm Biopharm. (2015) 96:11-21. doi: 10.1016/j.ejpb.2015.07.009.

[34] C. Argyo, V. Weiss, C. Bräuchle, T. Bein, Multifunctional Mesoporous Silica Nanoparticles as a Universal Platform for Drug Delivery, Chem. Mater. 26 (2014) 435–451. doi:10.1021/cm402592t.

[35] D.S. Goodsell, The molecular perspective: methotrexate, Stem Cells. (1999) 17(5):314-5.

[36] P.T. Wong, S.K. Choi, Mechanisms and implications of dual-acting methotrexate in folate-targeted nanotherapeutic delivery, Int J Mol Sci. 2015 16(1):1772-90. doi: 10.3390/ijms16011772.

[37] O.H. Clark, K. Levin, Q.H. Zeng, F.S. Greenspan, A. Siperstein, Thyroid cancer: the case for total thyroidectomy, Eur J Cancer Clin Oncol. (1988) 24(2):305-13.

[38] J. Seligmann, C. Twelves, Tubulin: an example of targeted chemotherapy, Future Med Chem. (2013) 5(3):339-52. doi: 10.4155/fmc.12.217.

[39] E.Y.H.P. Lee, W.J. Muller, Oncogenes and Tumor Suppressor Genes, Cold Spring Harb Perspect Biol. (2010) 2(10): a003236. doi: 10.1101/cshperspect.a003236

[40] T. Ozaki, A. Nakagawara, Role of p53 in Cell Death and Human Cancers. Cancers (Basel). (2011) 3(1): 994–1013. doi: 10.3390/cancers3010994

[41] K.I. Hilgendorf, E.S. Leshchiner, S. Nedelcu, M.A. Maynard, E. Calo, A. Ianari, L.D. Walensky, J.A. Lees, The retinoblastoma protein induces apoptosis directly at the mitochondria. Genes Dev. (2013) 27(9):1003-15. doi: 10.1101/gad.211326.112

[42] I. Paatero, E. Casals, R. Niemi, E. Özliseli, J.M. Rosenholm, C. Sahlgren, Analyses in zebrafish embryos reveal that nanotoxicity profiles are dependent on surface-functionalization controlled penetrance of biological membranes. Sci Rep. (2017) 7(1):8423. doi: 10.1038/s41598-017-09312-z.L.

[43] J. Marrison, L. Räty, P. Marriott, P. O'Toole, Ptychography--a label free, high-contrast imaging technique for live cells using quantitative phase information. Sci Rep. (2013) 3:2369. doi: 10.1038/srep02369.

[44] Kroemer G, Galluzzi L, Vandenabeele P, Abrams J, Alnemri ES, Baehrecke EH, Blagosklonny MV, El-Deiry WS, Golstein P, Green DR, Hengartner M, Knight RA, Kumar S, Lipton SA, Malorni W, Nuñez G, Peter ME, Tschopp J, Yuan J, Piacentini M, Zhivotovsky B, Melino G; Nomenclature Committee on Cell Death 2009. (2009). Classification of cell death: recommendations of the Nomenclature Committee on Cell Death 2009. Cell Death Differ. 16(1):3-11. doi: 10.1038/cdd.2008.150.

[45] N. Kramer, A. Walzl, C. Unger, M. Rosner, G. Krupitza, M. Hengstschläger, H. Dolznig, In vitro cell migration and invasion assays. Mutat Res. (2013) 752(1):10-24. doi: 10.1016/j.mrrev.2012.08.001.

[46] C.R Justus, N. Leffler, M. Ruiz-Echevarria, L.V. Yang, In vitro cell migration and invasion assays. J Vis Exp. (2014) (88). doi: 10.3791/51046.

[47] D. Bhakta-Guha, T. Efferth, Hormesis: Decoding Two Sides of the Same Coin. Pharmaceuticals (Basel). (2015) 8(4):865-83. doi: 10.3390/ph8040865.

[48] L. Ossowski, E. Reich, Experimental model for quantitative study of metastasis. Cancer Res. (1980) 40(7):2300-9.

[49] M. Zeisser-Labouèbe, F. Delie, R. Gurny, N. Lange, Screening of nanoparticulate delivery systems for the photodetection of cancer in a simple and cost-effective model. Nanomedicine (Lond). (2009) 4(2):135-43.

[50] P. Nowak-Sliwinska, T. Segura, M.L. Iruela-Arispe, The chicken chorioallantoic membrane model in biology, medicine and bioengineering. Angiogenesis. (2014) 17(4):779-804. doi: 10.1007/s10456-014-9440-7.

[51] N.A. Lokman, A.S. Elder, C. Ricciardelli, M.K. Oehler, Chick chorioallantoic membrane (CAM) assay as an in vivo model to

study the effect of newly identified molecules on ovarian cancer invasion and metastasis. Int J Mol Sci. (2012) 13(8):9959-70. doi: 10.3390/ijms13089959.

[52] N. Bergelin, C. Löf, S. Balthasar, V. Kalhori, K. Törnquist, S1P1 and VEGFR-2 form a signaling complex with extracellularly regulated kinase 1/2 and protein kinase C-alpha regulating ML-1 thyroid carcinoma cell migration. Endocrinology. (2010) 151(7):2994-3005. doi: 10.1210//en.2009-1387.

[53] J.E. Grey, S. Enoch, K.G. Harding, Wound assessment. BMJ. (2006) 332(7536):285-8.S.

[54] S. Sotiriou, N. Koletsas, T. Koletsa, S. Touloupidis, M. Lambropoulou,Thyroid transcription factor-1 expression in invasive and non-invasive urothelial carcinomas. Hippokratia. (2017) 21(3):154-157.

[55] M. Lamba Saini, C. Bouzin, B. Weynand, E. Marbaix, An Appraisal of Proliferation and Apoptotic Markers in Papillary Thyroid Carcinoma: An Automated Analysis. PLoS One. (2016) 11(2):e0148656. doi: 10.1371/journal.pone.0148656.

[56] C.Y. Liu, H.H. Lin, M.J. Tang, Y.K. Wang, Vimentin contributes to epithelial-mesenchymal transition cancer cell mechanics by mediating cytoskeletal organization and focal adhesion maturation. Oncotarget. (2015) 6(18):15966-83.

[57] J. Rosenholm, A. Penninkangas, M. Lindén, Amino-functionalization of large-pore mesoscopically ordered silica by a one-step hyperbranching polymerization of a surface-grown polyethyleneimine. Chem Commun (Camb) (2006) (37):3909-11.

[58] J. Rosenholm, A. Duchanoy, M. Lindén, Hyperbranching Surface Polymerization as a Tool for Preferential Functionalization of the Outer Surface of Mesoporous Silica. Chem Mater. (2008) 1126–1133. doi: 10.1021/cm7021328.

[59] C.A. Schneider, W.S Rasband, K.W. Eliceiri, NIH Image to ImageJ: 25 years of image analysis. Nat Methods. (2012) Jul;9(7):671-5.

[60] I. Nicoletti, G. Magliorati, M. Pagliacci, F. Grignani, C. Riccardi, A rapid and simple method for measuring thymocyte apoptosis by propidium iodide staining and flow cytometry. J Immunol Methods (1991) 139.

[61] J.M. Rosenholm, E. Peuhu, L.T. Bate-Eya, J.E. Eriksson, C. Sahlgren, M. Lindén, Cancer-cell-specific induction of apoptosis using mesoporous silica nanoparticles as drug-delivery vectors. Small. (2010) 6(11):1234-41. doi: 10.1002/smll.200902355.

[62] H.S. Leong, K.S. Butler, C.J. Brinker, M. Azzawi, S. Conlan, C. Dufès, A. Owen, S. Rannard, C. Scott, C. Chen, M.A. Dobrovolskaia, S.V. Kozlov, A. Prina-Mello, R. Schmid, P. Wick, F. Caputo, P. Boisseau, R.M. Crist, S.E. McNeil, B. Fadeel, L. Tran, S.F. Hansen, N.B. Hartmann, L.P.W. Clausen L.M. Skjolding, A. Baun, M. Ågerstrand, Z. Gu, D.A. Lamprou, C. Hoskins, L. Huang, W. Song, H. Cao, X. Liu, K.D. Jandt, W. Jiang, B.Y. Kim, K.E. Wheeler, A.J. Chetwynd, I. Lynch, S.M. Moghimi, A. Nel, T. Xia, P.S. Weiss, B. Sarmento, J. das Neves, H.A. Santos, L. Santos, S. Mitragotri, S. Little, D. Peer, M.M. Amiji, M.J. Alonso, A. Petri-Fink, S. Balog, A. Lee, B. Drasler, B. Rothen-Rutishauser, S. Wilhelm, H. Acar, R.G. Harrison, C. Mao, P. Mukherjee, R. Ramesh, L.R. McNally, S. Busatto, J. Wolfram, P. Bergese, M. Ferrari, R.H. Fang, L. Zhang, J. Zheng, C. Peng, B. Du, M.Yu, D.M. Charron, G. Zheng, C. Pastore, On the issue of transparency and reproducibility in nanomedicine. Nat Nanotechnol. 2019 Jul;14(7):629-635. doi: 10.1038/s41565-019-0496-9.

[63] P.B. Armstrong, J.P. Quigley, E. Sidebottom, Transepithelial Invasion and Intramesenchymal Infiltration of the Chick Embryo Chorioallantois by Tumor Cell Lines. Cancer Res. (1982) 42(5):1826-37.